ANNALES
UNIVERSITATIS MARIAE CURIE-SKLODOWSKA
LUBLIN — POLONIA
VOL. XLVI/XLVII, 34 SECTIO AAA 1991/1992

Department of Physics, Tampere University of Technology, Tampere (Finland)

M. PESSA

Quantum Well Lasers and Avalanche Photodetectors

INTRODUCTION

Molecular beam epitaxy (MBE), gas-source MBE, chemical beam epitaxy (CBE), and metalorganic chemical vapor deposition (MOCVD) methods have demonstrated their ability to produce the best state-of-art materials for advanced photonic and electronic devices [1–4]. Not only lattice-matched heteroepitaxy but also growth of pseudomorphic (coherent) lattice-mismatched layers are possible by these methods in a closely controlled manner.

The most developed low-dimensional semiconductor structures are these based on abrupt heterostructures between GaAs and $Al_xGa_{1-x}As$. This material system depends for its success on the close match between the two binary compounds, GaAs and AlAs, which have almost the same lattice parameters and thermal expansion coefficients. Another useful lattice-matched system for device applications is $InP/In_xGa_{1-x}As_yP_{1-y}$.

Development in optoelectronics has created demands for new materials and device concepts. A variety of new devices are now emerging where the constituent layers are deliberately chosen to be grossly mismatched. Discovery of pseudomorphic growth has significantly contributed to the development of photonic devices, notably quantum well (QW) lasers. A typical mismatched structure is $In_xGa_{1-x}As$/-InGaAsP ($x \neq 0.53$), used for strained QW lasers for fiber optical communication at $\lambda \approx 1.5$ μm and for Er-doped fiber amplifiers (EDFA) at $\lambda \approx 1.48$ μm. Another mismatched structure is InGaAs/GaAs used for EDFA at $\lambda \approx 0.98$ μm. Introducing these coherently strained quantum wells in a laser structure positively affects the lasing properties. It is worth mentioning in passing that blue-light laser diodes, now capable of lasing at $\lambda < 500$ nm in pulsed mode up to 273 K, consist of strained $Zn_xCd_{1-x}Se$ quantum wells centered in ZnSe or ZnSSe barrier layers (see e.g. [5] and references therein).

The lattice-matched InGaAsP/InP heterostructure possesses a suitable energy band-gap for photon detection in the 1.0–0.6 μm wavelength region. The lattice-matched AlGaAs/GaAs system, on the other hand, is suitable for shorter wave-lengths, $\lambda < 0.9\mu$m, extending to the visible region where silicon has relatively poor responsivity. The crucial requirements to be met by these devices are (i) high quantum efficiency, (ii) low dark current, (iii) low capacitance, and (iv) low noise. These translate to stringet materials requirements, and lead to novel band-gap engineering to meet some of the criteria.

LASER DIODES

EFFECTS OF STRAIN ON QUANTUM WELLS OF LASERS

The lattice-mismatch induced axial strain of a zinc-blende structure like $In_xGa_{1-x}As$ splits the fourfould degenerate heavy hole (HH)$\pm 3/2$ valence state and light hole (LH) $\pm$ 1/2 valence state into double degenerate components [6,7] at the Brilloun zone center $k = 0$. Biaxial compression, generated if $x > 0.53$, in the plane of the quantum well shifts the HH bands to the valence band top. Biaxial tension, $x < 0.53$, shifts the LH bands to the valence band top. The energy difference between the HH and LH bands, $\Delta E_{hh} - \Delta E_{lh} = \delta E_{sh}$, the shear-component of strain, is directly observable by various optical methods. It is proportional to biaxial strain $\epsilon = \epsilon_{xx} = \epsilon_{yy} = (a_{QW} - a_B)/a_B$ via the equation $\delta E_{sh} = -2b(1 + 2C_{12}/C_{11})\epsilon$. The other components of strain are $\epsilon_{zz} = -2(C_{12}/C_{11})\epsilon$ and $\epsilon_{xy} = \epsilon_{yz} = \epsilon_{zx} = 0$. Here the ratio of elastic constants $C_{12}/C_{11} \approx 0.6$, b is the shear deformation potential, and $a_{QW,B}$ the lattice constant of the quantum well or the barrier layer. The hydrostatic component is defined as $\delta E_{hy} = -2c[(C_{11} - C_{12})/C_{11}]\epsilon$, where c is a deformation potential.

The effective HH mass $m*_{hh}$ in compressive strained quantum well is small, $0.089m_e$ compared to the bulk $m*_{hh} = 0.41m_e$ at Γ, reducing the density of states at the valence band maximum. Therefore, population inversion occurs at low injection carrier densities. This reduction in density of states together with a spliting of the hole sub-bands, which virtually eliminates the intervalence band absorption and two hole-electron Auger recombination (known to cause the major optical loss in 1.55 μm lasers), and an increase in the conduction band offset which diminishes the barrier leakage current, yield TE polarized lasing with low threshold current density (J_{th}), high external quantum efficiency (η_d), high differential gain (dg/dN), high output power (P), and closely controlled wavelength [8–11].

A biaxial tensile strained $In_xGa_{1-x}As$ quantum well can also have advantages over an unstrained quantum well [12], although no improvement is expected from the band structure calculation. The calculation predicts a larger effective mass of $2m_e$ for the top LH band under tensile strain, compared to $m*_{lh} \approx 0.065m_e$ of the unstrained bulk-like lattice, and a smaller sub-band splitting than that produced by compressive strain. However, experiments show that in fact the opposite is true. In particular, significant improvement has been found in J_{th}, dg/dN, line

enhancement factor α', and K factor for lasers with tensile strain quantum wells. Here $K = (\gamma\tau - 1)/(\tau f_0^2)$, γ is the damping rate of the relaxation oscillation frequency f_0 and τ is the carrier lifetime. The tensile strained QW lasers emit in TM mode. The improvement in laser action is attributed to the suppression of spontaneous emission associated with light polarization in the plane of quantum well and enhanced dipole moment associated with e-LH transitions, while it seems that the effects of large $m*_{lh}$ on gain (g) are not very dramatic.

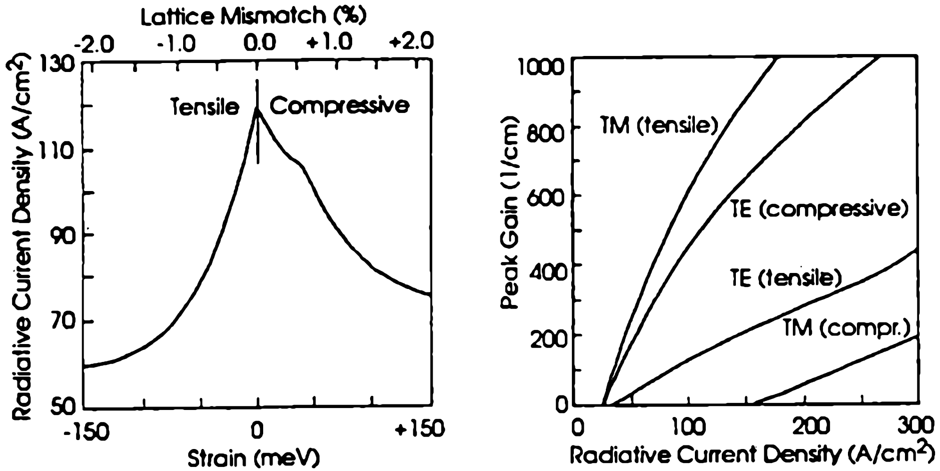

Fig. 1. Left panel: calculated radiative current density to achieve gain of 350 cm^{-1} as a function of lattice mismatch. Here strain of 1% is assumed to cause ΔE_{sh} of 70 meV (obtained from the above equation by setting $b \approx -1.5$). Right panel: peak gain for 20 nm wide QW layers under compressive and tensile strain of 100 meV (equivalent to about 1.5% lattice-mismatch) as a function of radiative current density. At this well width quantum confinement effects are small, and therefore the results can be deemed typical of bulk-like strained lattice

Fig. 1 shows radiative current densities needed to attain g of 350 cm^{-1} as a function of strain in InGaAs, and the peak gain variation as a function of radiative current density. Because the density of states at the valence band edge is approximately halved for bulk-like layers under biaxial tensile and compressive strain, transparency currents are expected to be about the same for the two cases of strain. However, dg/dN should be larger for the QW structure under tensile strain, due to a more favorable character of the valence band edge states. In other words, the line width enhancement factor

$$\alpha' = \frac{-4\pi dn/sN}{\lambda dg/dN}$$

(here, n — refractive index, N — carrier density) should also be more reduced for the tensionally strained structure than for the compressively strained structure, resulting in a smaller linewidth for single mode lasers. These predictions of theory have qualitatively been supported by many experiments, see e.g. [12,13], but any

precise quantitative comparison of the differences between the effects of tensile strain and compressive strain on laser action is difficult because of the scarcity of respective experimental data available.

LASERS FOR $\lambda = 1.5\mu m$

From the above discussion it is clear that any lattice strain in the quantum well lowers J_{th} from that of the lattice-matched case, provided that strain remains below its critical value for a given layer thickness. Experiments on InGaAs/InGaAsP lasers have revealed that J_{th} reaches its minimum at $x = 0.65 - 0.7$, corresponding to compressive strain of $0.8 < \epsilon < 1.2\%$, and at $x \approx 0.3$ corresponding to tensile strain of $\epsilon \approx -1.6\%$.

The smallest room-temperature threshold current densities reported to date [14], known to the author, for single-QW graded-index separate confinement heterostructure (GRIN-SCH) InGaAsP lasers are 186 A/cm^2 for compressive strain ($x = 0.65$) and 192 A/cm^2 for tensile strain ($x = 0.3$) with the cavity length L of 2 mm. For comparison, a lattice-matched ($x = 0.53$) QW laser of the same structure has exhibited J_{th} of 2 kA/cm^2 which, however, is unexpectedly high [14]. For further comparison, a 2-mm tensionally strained single-QW InGaAs/AlGaInAs GRIN-SCH laser [15], one of the latest phosphorus-free laser structures designed for emission at 1.5 μm, has yielded $J_{th} \approx 210$ A/cm^2.

Let us consider shorter cavities. The threshold current density rises when L is shortened, due to gain saturation of the quantum well since mirror loss becomes dominant. This phenomenon is expected to be expecially prominent for tensile strained QW lasers because the facet reflectivity for dominant TM mode is low. At $L = 1$ mm, $480 < J_{th} < 500$ A/cm^2 has been demonstrated for four-QW GRIN--SCH InGaAs/InGaAsP lasers [16,17] with $0.6 < x < 0.62$. This J_{th} is about one half of $770 < J_{th} < 1100$ A/cm^2 obtained for the best unstrained four--QW GRIN--SCH InGaAs/InGaAsP lasers of the same length [18,19]. For $0.4 < L < 0.5$ mm, $1500 < J_{th} < 2000$ A/cm^2 has been achieved for a lattice-matched four-QW GRIN--SCH InGaAs/InGaAsP laser [18,19]. It should be noted that J_{th}'s of a single-QW laser and multiple QW laser of the same structure are not directly comparable with each other. A "thumb rule" is that adding one quantum well in the active region costs roughly 100 A/cm^2 in J_{th}; hence, the single-QW and four-QW strained lasers discussed above are almost identical in quality.

Very low threshold current densities of QW InGaAs/InGaAsP lasers, prepared by CBR, gas-source MBE, and MOCVD are presented in Fig. 2.

To further illustrate the performance of state-of-the-art lasers for emission at $\lambda = 1.5$ μm we present L-I characteristics of 0.15 mm long QW InGaAs/InGaAsP lasers processed to semi-insulating planar buried heterostructures (SIPBH), see Fig. 3. These devices are capable of operating at sub-mA threshold currents at 10°C. Also shown in Fig. 3 is the L-I curve of a 1 mm long two-QW InGaAs/-InGaAsP-SIPBH laser with AR/HR facet coatings. This laser exhibits a record cw output power of 325 mW at room temperature [14].

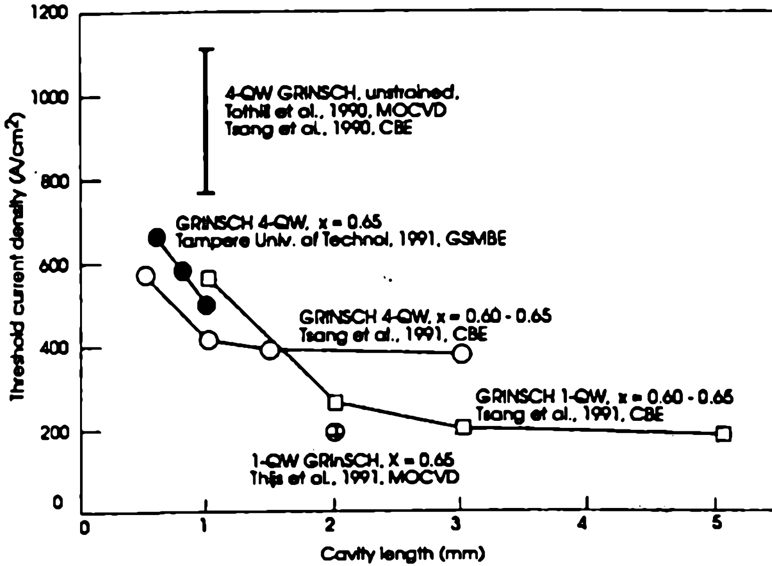

Fig. 2. Very low threshold current densities of QW InGaAs/InGaAsP GRIN-SCH quantum well lasers, grown by various methods, as a function of cavity length [14,17,20]. Also shown are threshold current densities for unstrained 4-QW InGaAs/InGaAsP GRIN-SCH lasers [18,19]

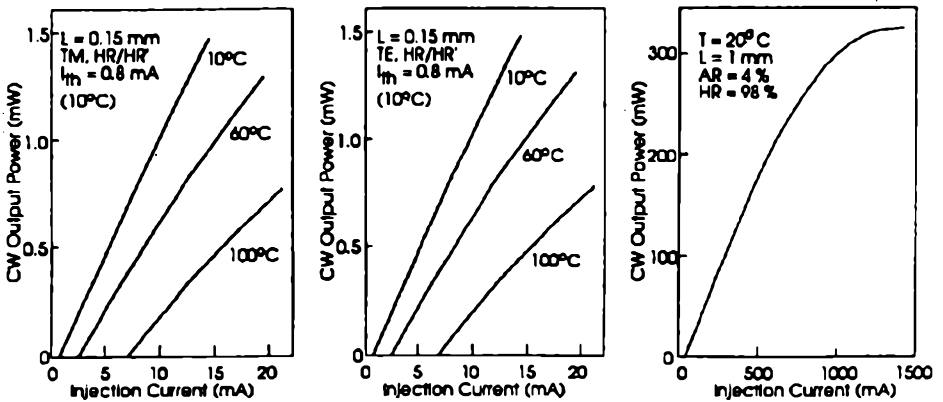

Fig. 3. CW light-output for 1.6% tensionally strained single-QW InGaAs/InGaAsP-SIPBH laser (left panel), for a 1.2 compressively strained two-QW InGaAs/InGaAsP-SIPBH laser (middle panel) at different operating temperatures, and for a 1.2% compressively strained four-QW InGaAs/InGaAsP-SIPBH laser at room temperature (right panel) [14]

The internal quantum efficiency η_i and internal propagation loss α_i, are related to each other by

$$\frac{1}{\eta_d} = \frac{1}{\eta_i}\left(1 + \frac{\alpha_i L}{\ln(1/R)}\right),$$

where R denotes the reflectivity of the cleaved facets, η_d is external quantum efficiency, α is cavity length. By plotting $1/\eta_d$ against L a linear function is obtained from the slope and intercept of which it is possible to derive η_i and α_i. As typical values of η_i and α_i for perhaps the most common four-QW InGaAs/InGaAsP GRIN-SCH lasers we present our results, namely, $\eta_i \approx 57\%$ and $\alpha_i \approx 6$ cm^{-1}. The temperature dependence of threshold current I_{th} is represented by the expression $I_{th} = I_0 e^{T/T_0}$. The characteristic temperature T_0 of such lasers is usually between 60 and 70 K, T_0 being rather independent of the degree and sign of strain in the temperature interval from 10 to 60°.

The cw output power at room temperature for strained 2–4 μm wide 0.5–1.0 mm long ridge waveguide SCH QW lasers normally ranges from 20 to 50 mW per facet at the highest injection current possible. Application of AR/HR facet coating increases P very remarkably. At present, maximum P seems to culminate at 325 mW for a compressive laser, as mentioned above. Tensile strained ($x = 0.3$) lasers exhibit somewhat lower P_{max}, the best reported values are about 150 mW. These high output powers are to be compared with p_{max} = 110 mW for the best 1-mm unstrained five-QW lasers which are made of a buried ridge stripe structure and with P_{max} = 70 mW for conventional "bulk" lasers [21]. The latter two lasers have approximately the same architecture and AR/HR facet coating.

Although higher P is produced from compressive QW InGaAs/InGaAsP lasers than from tensile QW InGaAs/InGaAsP lasers of the same structure, the latter may be more suitable for high-speed applications. They seem to have slightly higher dg/dN and smaller α', as already mentioned, and smaller K than those of compressive QW lasers. Factor K, which was earlier defined in terms of f_0, can also be expressed in terms of maximum intrinsic modulation bandwidth f_{max} as $K = (2\sqrt{2})\pi/f_{max}$. The smallest K, 0.22 ns, reported for tensile strained ($x = 0.3$) four-QW GRIN-SCH-SIPBH InGaAsP/InGaAsP lasers implies very high f_{max} of 40 GHz [14]. For compressive strained ($x = 0.7$) four-QW GRIN-SCH--SIPBH InGaAsP/InGaAsP lasers K of 0.58 ns has been attained, corresponding to f_{max} = 15 GHz.

We mentioned in passing that the RACE program, a major European Communitiy action aimed at integrated broadband telecommunications, has taken full benefit of QW technology described above within the Advanced QW Lasers for Multigigabit Transmission System Project (RACE-I AQUA). The AQUA team has demonstrated a successful application of multiple QW-DFB-SIBH lasers for 10 GBit/s transmission systems [22,23]. A low threshold current of 7 mA on 400 μm long devices without facet coating, an output power of 11 mW per facet at the drive current of 100 mA, a sidemode suppression of 33 dB under 10 GBit/s NRZ modulation, and the total chip capacitance of 2.6 pF have been achieved. Moreover, using multiple QW-DFB-BRS facet coated lasers cw $P_{max} \approx 110$ mW has been demonstrated.

LASERS FOR $\lambda = 0.98\ \mu m$

The optimum pump wavelength for the EDFA is 0.98 μm produced from a strained QW $In_xGa_{1-x}As/GaAs/Al_yGa_{1-y}As$ laser. Another suitable pump wavelength is 1.48 μm produced from a strained QW InGaAs/InGaAsP laser with a very similar structure to that of a 1.55-μm laser. However, excitation of Er--atoms with greater λ-disparity between the pump and the signal radiation obtainable by the by InGaAs/GaAs/AlGaAs laser reduces tolerances in the requisite dichroic elements of the EDFA. Also, Auger recombination in this material system is small, resulting in high T_0 and high g. It is also essential for an EDFA that the fiber coupling efficiency is good. This coupling requirement is met if operation in the fundamental transverse mode is maintained at a high light power level and if a large portion of the power emitted to free space is coupled into the fiber.

An $In_xGa_{1-x}As$ layer sandwiched between GaAs or AlGaAs layers always remains under biaxial compressive strain; the higher the strain, the better laser action is obtained. The maximum amount of indium is 25% for pseudomorphic growth of a quantum well not much thicker than 6 nm.

A record J_{th} of 56 Acm^2 on a 3 mm long single-QW GRIN-SCH $In_xGa_{1-x}As$/-$GaAs/Al_yGa_{1-y}As$ laser, where $x = 0.2$ and $y = 0.7$, has been achieved [24] with high $\eta_i \approx 88\%$ and low $\alpha_i \approx 1.8$ cm^{-1}. Typically, ridge waveguide QW lasers without AR/HR coating exhibit $\eta_d = 0.25$ to 0.35 mW/mA per facet (40 to 55%) for L ranging from 1 to 0.5 mm, respectively, and $T_0 = 80$–120 K. Applying AR/HR coating raises η_d to 0.5–0.0 mW/mA and T_0 to 160 K in the best cases. The are usually capable of oscillating in a single mode up to 30–40 mW (cw) per facet at 300 K. AR/HR coating increases cw power well over 100 mW for $L = 0.7$–1.0 mm. Recently, fundamental transverse mode operation at 200 mW, and maximum power of 385 mW, have been achieved on a 0.5 mm long two--QW InGaAs/GaAs/AlGaAs SCHO-BH laser consisting of $In_{0.5}Ga_{0.5}P$ and GaAs blocking layers [26].

Recently, a novel periodic index SCHI 5-μm wide 750 μm long self-aligned ridge--waveguide laser has been fabricated [25]. It emitted $P_{max} \approx 620$ mW in cw mode at room temperature. The η_d value was as high as 1.15 mW/mA (90%), and the coupling efficiency was 51% of free space emission into a lensed fiber of 5 μm core diameter at the maximum coupled power level of 130 mW.

Direct modulation 3 dB bandwidth of 19.5 GHz has been reported on 4 μm, wide, 200 μm long four-QW GRIN-SCH ridge structures [27]. A similar very high modulation bandwidth of 20 GHz, at over 20 mW power level and $K = 0.17$ ns, has also been reported for a $2 \times 140\ \mu m^2$ three-QW SCH-BH ridge waveguide laser [28].

It has been proposed [29] that replacing the AsGaAs cladding layer by a InGaP layer, lattice-matched to GaAs at $x = 49\%$, would make it easier to reproducibly process the devices, because selective chemical etching between GaAs and InGaP is possible. The use of InGaP should also improve long-term performance of the lasers for several reasons. Namely, the Al-free lasers tend to form less surface oxidation during fabrication process and laser operation; the oxidation-induced

facet degradation is the major failure mechanism. They possess a low surface recombination velocity, enhancing the catastrophical optical damage threshold and reducing leakage current.

The first cw room-temperature multiple QW InGaP/GaAs/InGaAs laser was grown by using gas-source MBE at AT&T Bell Laboratories in 1991 [30]. Broad--area lasers (L = 1 mm) exhibited J_{th} of 177 A/cm^2 and η_i of 91%. They lased at λ = 1017 nm. The characteristic temperature of 150 K obtained for 0.508 mm long lasers is among the highest values ever reported. With a 5×508 μm^2 ridge waveguide structure these lasers had I_{th} = 17.5 mA, η_d = 0.44 mW/mA per facet, and $\alpha_i \approx$ 9.1 cm^{-1}. In a more recent paper, the same research group reported several improvements [31]. A patterned n-type InGaP confinement layer was used to provide index guiding and current blocking. The threshold current was lowered to 12 mA for a AR/HR coated 2.5×508 μm^2 laser showing η_d = 0.68 mW/mA. The peak optical power up to 83 mW was attained from a 4.5×508 μm^2 laser before catastrophic optical damage at facets. The far-field pattern showed an angle of 54° in the transverse direction (perpendicular to the layers) and 19° in the lateral direction. The 2.5×508 μm^2 lasers showed a single mode suppression ratio more than 30 dB. Other parameters were T_0 = 130 K, $\eta_i \approx$ 82% and $\alpha_i \approx$ 11.9 cm^{-1}.

The Tampere group [32] has also grown InGaP/GaAs/InGaAs lasers by gas-

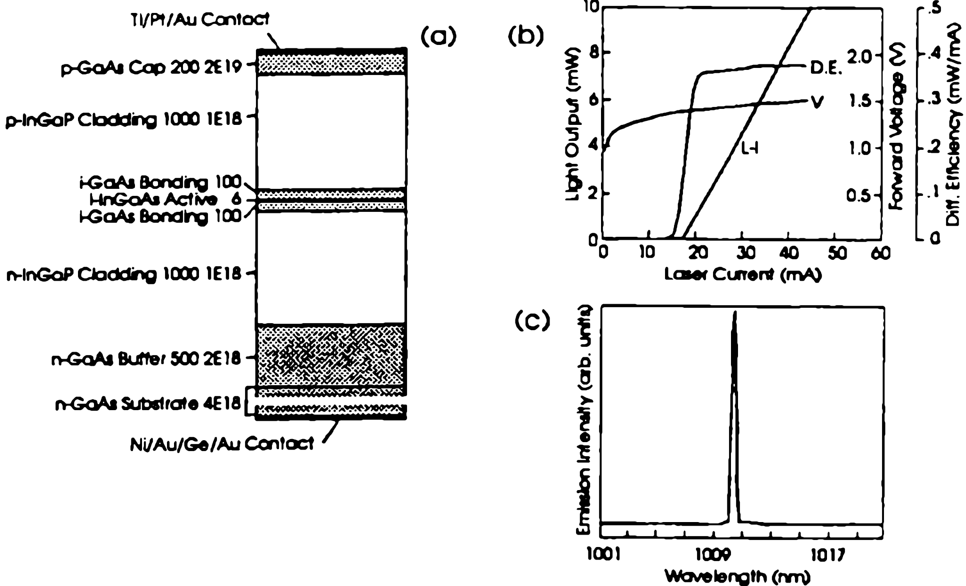

Fig. 4. (a) Schematic layer structure of gas-source MBE grown single-QW InGaAs/GaAs/-InGaAs SCH laser. (b) L–I characteristics, differential efficiency, and forward voltage. (c) Emission spectrum of a 0.4 mm long 4 μm wide single-QW ridge-waveguide laser operated in cw mode at room temperature. Numbers presented in the internal description of the panel (a) represent a thickness of layer in nm and a concentration of dopants in cm^{-3}

-source MBE. Preliminary tests on 1200 μm broad-area lasers have given J_{th} = 72 A/cm^2, $\alpha_i \approx 9.1$ cm^{-1}, $T_0 = 120 - 140$ K and $\eta_i = 0.3$ mW/mA per facet.

The first ridge-waveguide single-QW InGaP/GaAs/InGaAs laser test results obtained by us are shown in Fig. 4. The 3×400 μm^2 ridge-waveguide lasers operated in cw mode at room temperature exhibit I_{th} = 18–20 mA, η_d = 0.35–0.38 mW/mA per facet, $\lambda = 1005 - 1010$ nm, and the far-field pattern of about 51° × 12°. By reducing the InGaAs layer thickness, or In concentration in this layer, the lasers would operate at the desired resonance peak wavelength of 0.982–0.985 μm for an efficient excitation of Er^{+3} ions in the fiber.

AVALANCHE PHOTODETECTORS

GENERAL CONSIDERATIONS

Avalanche photodetectors internally amplify the primary photocurrent and are good candidates for low optical power detection. However, the multiplication process is intrinsically noisy because of statistical nature. In order to reduce noise it is necessary to have an APD structure where the ionization rates of electrons (α_e) and holes (β_h) differ from each other as much as possible.

The APDs that have shown the most promise for low noise, high gain, and high frequency operation consist of separate regions for absorption, graded-E_g, and multiplication (SA(G)M). A number of various SA(G)M-ADP structures have been fabricated in an attempt to find an optimized structure where the gain--bandwidth product (GB) would be maximized with the smallest possible penalty in multiplication noise figure.

A general expression for the frequency dependent multiplication M(ω), valid for SAM-APDs, is

$$\frac{M(\omega)}{M_0} = T(\omega)\left[(1+\frac{\omega^2}{e_h^2})(1+\omega^2R^2C^2)(1+\omega^2\tau_e^2M_0^2)\right]^{-1/2}$$

Here ω is the angular frequency, M_0 the multiplication factor at zero frequency, $T(\omega)$ a transit-time factor, e_h the emission rate of holes trapped at the hetero-junction interfaces, R the series resistance, C the diode capacitance, and τ_e the effective transit time of electrons through the multiplication region. For an optimum frequency response the capacitance should be minimized, carrier generation be avoided in non-depleted regions to prevent slow diffusion of carriers, drift distances be mimized, and trapping be reduced by smoothing heterojunctions employing a grading layer.

SAM-APDs operating at gain M has a shot noise current, multiplied by a gain dependent excess noise factor F, i.e.,

$$\langle i_s^2\rangle = 2e(I_p + I_b + I_d)M^2FB.$$

Here e is electron charge, I_b is the photocurrent generated by background radiation, I_d is the dark current, I_p is current density and B is the shot noise bandwidth.

Noise characteristics of APDs can be measured and the ratio $k = \beta_h/\alpha_e$ be determined. The ionization coefficients β_h and α_e strongly depend on the electric field applied. It is customary to compare the noise measurements data with the F factor using the equation

$$F = M\left[1 - (1-k)\frac{(M-1)^2}{M^2}\right]$$

for pure electron injection. It can be seen that to minimize $\langle i_s^2 \rangle$, I_d and k must be minimized because at high multiplication $F \rightarrow kM$. Unfortunately, k is nearly equal to 1 for the III–V compound semiconductors, as opposed to Si for which $k \approx 0.1$. Therefore, Si APDs are excellent devices for detection at $\alpha < 1.1$ μm, although they have relatively poor response in the blue-light region. An advantage of III–V semiconductor APDs over silicon APDs is the tunability of the E_g and k by applying band-gap engineering [33–35].

APDs FOR FIBER OPTICAL COMMUNICATON

The ever-expanding telecommunications marketplace has stimulated efforts to increase the circuit capacity of lightwave systems. A rapid increse in the rate of transmission has led to the multi-Gb/s era, with high receiver sensitivities having been realized by a careful optimization of the APD structure for multi--GHz bandwidths. To date, the structure that has shown the most promise for high frequency operation is an InP/AnGaAsP/InGaAs SAGM-APD. In this and similar APDs absorption of photons takes place in a narrow-gap i-$In_{0.53}Ga_{0.47}As$ layer, while multiplication takes place in a wide-gap relatively thin InP layer which may be lightly doped because otherwise the electric field in InGaAs will be too high ($\geq 2 \times 10^5$ V/cm) and cause tunnelling that leads to excess dark current. The multiplication region and the absorption region in SAGM is separated by a transition region comprised of several intermediate band-gap $In_xGa_{1-x}As_{y-1}P$ layers.

State-of-the-art InGaAs(P)/InP SA(G)M-APDs for high-speed optical communication systems show GB of over 60 GHz. At the same time I_d has been kept low, between 10 nA and 110 nA, depending on the device structure employed, measured at 90% of the reverse breakdown voltage V_{break}. Operation of these devices at $10 < M < 20$ is found suitable for the detection of high-speed modulated light [36–38].

Fig. 5 shows one of the most successful CBE-grown SAGM-APD structure and the dark current and avalanche gain versus bias voltage [35, 38, 39]. This quite high level of I_d is due to doping InP to a considerable level ($n_d \approx 5.5 \times 10^{16}$) cm^{-3} which is neccessary to achieve high GB products. In the same diagram we show our gas-source MBE grown InP/InGaAs SAM-APD for comparison. Here, the multiplication region is relatively thick (1 μm) and undoped (low-10^{15} cm^{-3}),

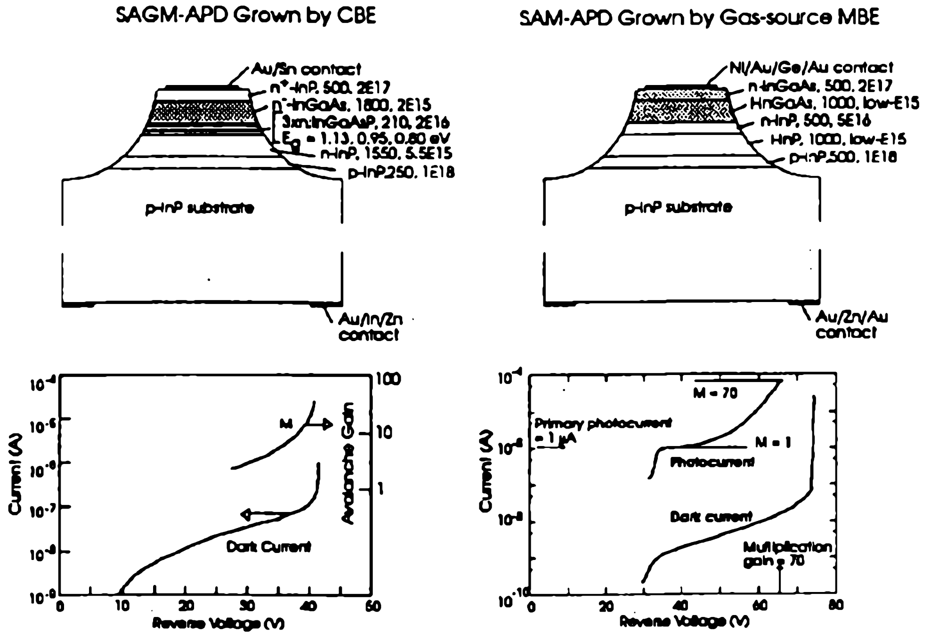

Fig. 5. Cross-section of SAGM-APD [35] and SAM-APD [40], and the dark current and avalanche gain plotted against reverse bias voltage. Numbers presented in internal description of APD cross--section represent the thickness of layer in nm and the concentration of dopants in cm^{-3}

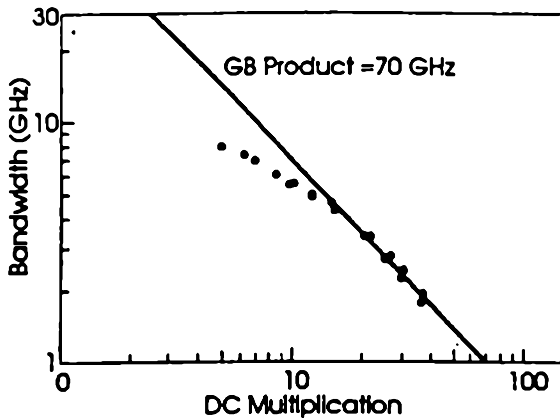

Fig. 6. Bandwidth plotted against DC avalanche gain for the SAGM-APD shown in Fig. 5

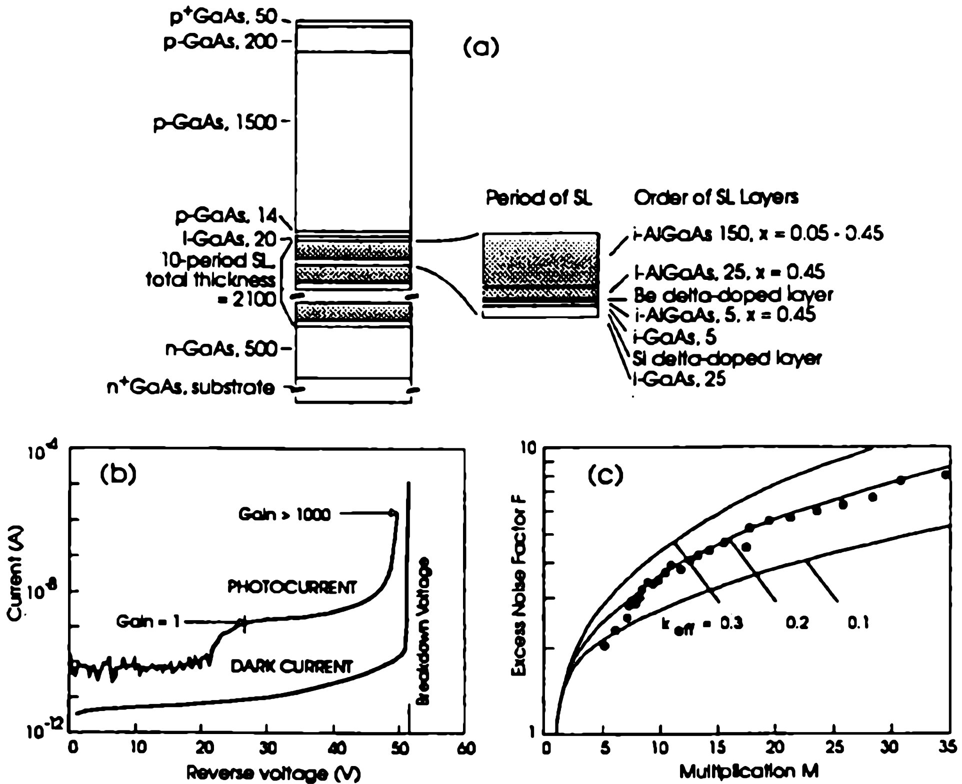

Fig. 7. (a) Schematic layer structure of MBE grown δ-doped staircase AlGaAs/GaAs separate absorbion and multiplication avalanche photodetector. Number in internal description of panes (a) represent the thickness of layer in nm. (b) Photocurrent and dark current of a 150-μm dia mesa diode. (c) Excess noise factor as a function of multiplication [41]

yielding remarkably good values for M and I_d. We obtain $M = 70$ and $I_d = 17$ nA at 90% of V_{break} for this device of a 150 μm mesa diameter [40]. This I_d suggests that the primary unmultiplied dark current, I_d/M, is only about 0.24 nA which, in turn, is indicative of low density of interace defects and accurate lattice-matching, but it is likely than the GB product of our device (not measured) remains smaller than the GB of SAGM-APD.

Fig. 6 displays the bandwidth of the SAGM-APD of Fig. 5 as a function of DC avalanche gain. In the high-gain regime, $M_0 \geq 15$, the device response is limited by the gain-bandwidth, the constant GB product being as high as 70 GHz. In the low-gain regime, the bandwidth is determined by a combination of the RC constant, trapping of holes at the interfaces, and the transit time of carriers through the depletion region, resulting in a maximum bandwidth of 8 GHz.

APDs FOR VISIBLE LIGHT

We have developed SAM-APDs for detecting very weak photon fluxes in visible light [41]. To reduce k and increase M, "staircase" AlGaAs/GaAs superlattice (SL) structures have been prepared. Fig. 7 shows one of our best SAM-APDs, consisting of p-type and n-type δ-doped layers in each period of the 10-period graded-E_g SL. Such a staircase SL is inserted in the i-region of a basic p-i-n structure to produce a high electric field in the multiplication region and small threshold for the hot electrons. The purpose of δ-doped dipoles is to heat the electrons when they pass through the AlGaAs/GaAs interfaces in the SL so that the probability for ionization would be increased. The δ-doped sheet concentrations must match each other in order to produce a uniform electric field profile in the SL and to diminish the depletion voltage of the structure.

Fig. 7 summarizes the results obtained for the complex staircase SL SAM--APD [41]. This mesa diode has a light sensitive area of 150 μm in diameter and a 0.065 mm^2 total cross-sectional area. The dark current is less than 100 pA up to a very abrupt breakdown voltage, indicative of the absence of tunnelling in the absorbing layer. The photocurrent is small at bias values below 22 V because the structure in not completely depleted, resulting in low probability (ξ) for generation of an electron-hole pair by a single photon. At about 25 V, ξ becomes saturated and M equals ≈ 1. The increase in photocurrent beyond 25 V is due to an increase in M, yielding extremely high $M > 1000$ near V_{break}. It is also worth noticing that small $k \leq 0.2$ forces the excess noise factor to remain below 10 throughout the range from $M = 1$ to 35, which further demonstrates the superiority of this type of photodectector to any "bulk-like" III–V semiconductor photodetector.

ACKNOWLEDGEMENTS

This work was supported by Technology Development Centre (TEKES, Finland), Academy of Finland, DCA Instruments Ltd., Wallac Ltd., and Tampere University of Technology.

REFERENCES

[1] Cho A., *J. Cryst. Growth*, 95 (1989), 1.

[2] Pessa M., Hakkarainem T., Keskinen J., Rakennus K., Salokatve A., Zhang G., Asonen H., *SPIE*, 1362 (1991), 529.

[3] Tsang W. T., *J. Cryst. Growth*, 105 (1990), 29.

[4] Razeghi M., *The MOCVD Challenge*, vol. 1, *A Survey of GaInAsP-InP for Photonic and Electronic Applications*, Adam Holger, Bristol 1989.

[5] Pessa M., Ahn D. [in:] *II–VI Compound Semiconductors*, (ed.) M. Jain, World Scientific Publ. Co., to be published in 1992.

[6] Yablonovitch E., Kane E. O., *J. Lightwave Technol.*, 6 (1988), 1292.

[7] O'Reilly E. P., Jones G., Ghiti A., Adams A. R., *Electron. Lett.*, 27 (1991), 1417.

[8] Zah C. E., Bat R., Pathak B., Caneau C., Favire F. J., Andreadakis N. C., Hwang D. M., Koza M. A., Chen C. Y., Lee T. P., *Electron. Lett.*, 27 (1991), 1414.

[9] Thijs P. J. A., Montie E. A., van Dongen T., Bulle-Lieuwma C. W. T., *J. Cryst. Growth*, 105 (1990), 339.

[10] Thijs P. J. A., van Dongen E., *Electron. Lett.*, 25 (1989), 1735.

[11] Temkin H., Tanbundek T., Logan R. A., *Appl. Phys. Lett.*, 56 (1990), 1210.

[12] Tiemeijer L-F., Thijs P. J. A., de Waard P. J., Binsma J. J., van Dongen T., *Appl. Phys. Lett.*, 58 (1991), 2738.

[13] Tanbun-Ek T., Olsson N. A., Logan R. A., Wecht K. W., Sergent A. M., *IEEE Photonics Technol. Lett.*, 3 (1991), 1041.

[14] Thijs P. J. A., Binsma J. J. M., Tiemeijer L-F., van Dongen T., *ECO91-IOOC, Paris, Sept. 9-12, 1991*; Thijs P. J. A., Tiemeijer L-F., Kuindersma P. I., Binsma J. J. M., van Dongen T., *IEEE J. Quantum Electron.*, 27 (1991), 1426.

[15] Kasukawa A., Bhat R., Zah C. E., Koza M. A., Lee T. P., *Appl. Phys. Lett.*, 59 (1991), 2486.

[16] Temkin H., Tanbun-Ek T., Logan R. A., Cebula D. A., Sergent A. M., *IEEE Photonics Technol. Lett.*, 3 (1991), 100.

[17] Asonen H., Keskinen J., Näppi J., Koteoja M., Tappura K., Rakennus K., Hakkarainen T., Pessa M., *EURO MBE-91, Tampere, Finland, April 21-14, 1991.*

[18] Tothill J. N., Wilkie J. H., Westbrook L., Hatch C. B., Halliwell M. A. G., Lyons M. H., *J. Electron. Materials*, 19 (1990), 515.

[19] Tsang W. T., Wu M. C., Yand L, Chen Y. K., Sergent A. M., *Electron. Lett.*, 26 (1990), 2036.

[20] Tsang W. T., Choa F. S., Wu M. C., Chen Y. K., Sergent A. N., Sciortino Jr. P. F., *Appl. Phys. Lett.*, 58 (1991), 2610.

[21] Kazimierski C., Ougazzaden A., Blez M., Robein D., Landreau J., Sermage B., Bouley J. C., Mircea A., *IEEE J. Quantum Electron.*, 6 (1991), 1794.

[22] Speier P., *Intern. Conf. on InP and Related Compounds, Cardiff, April 8-13, 1991.*

[23] Speier P., Bouayad-Amine J., Cebulla U., Dütting K., Klenk M., Mayer H. P., Weinmann R., Wünstel K., Zielinski E., Hildebrand O., *Electron. Lett.*, 27 (1991), 863.

[24] Williams R. L., Dion M., Chatenound F., Dzurko K., *Appl. Phys. Lett.*, 58 (1991), 1819.

[25] Wu M. C., Chen Y. K., Hong M., Mannaerts J. P., Chin M. A., Sergent A. M., *Appl Phys. Lett.*, 59 (1991), 1046.

[26] Fukagai K., Ishikawa S., Fujii H., Endo K., *ECOC-91-IOOC, Paris, Sept. 9-12, 1991.*

[27] Offsey S. D., Lester L. F., Schaff W. J., Eastman L. F., *Appl Phys. Lett.*, 58 (1991), 2336.

[28] Hagarajan R., Fukushima T., Bowers J. E., Geels R. S., Coldren L. A., *Appl. Phys. Lett.*, 58 (1991), 2326.

[29] Ijichi T., Ohkubo M., Matsumoto N., Okamoto H., *12th IEEE Internat. Semicon. Laser Conf., Davos, Switzerland, Sept. 9-14, 1990*, Paper D-2, 44-45.

[30] Kuo J. M., Chen Y. K., Wu M. C., Chin M. A., *Appl. Phys. Lett.*, 59 (1991), 2781.

[31] Chen Y. K., Wu M. C., Kuo M. C., Chin M. A., Sergent A. M., *Appl. Phys. Lett.*, 59 (1991), 2929.

[32] Zhang G., Näppi J., Vättinen K., Asonen H., to be published in *Appl. Phys. Lett.*, 1992.

[33] Bhattacharya P., *Int. J. Optoelectr.*, 5 (1991), 51.

[34] Ripamonti G., Capasso F., Hutchinson A. L., Muehiner D. J., Walker J. F., Malik R. J., *Nucl. Inst. Methods Phys. Res.*, A 288 (1990), 99.

[35] Campbell J. C., Tsand W. T., Qua G. J., Bowers J. E., *Appl. Phys. Lett.*, 51 (1987), 1454.

[36] Kuebart W., Eisele H., Scherb J., Kimmerle J., Wiedemann P., Körber W., *ECOC'91-IOOC, Paris, Sept. 9-12, 1991.*

[37] Kuwatsuka H., Kito Y., Uchida T., Mikawa T., *ECOC'91-IOOC, Paris, Sept. 9-12, 1991.*

[38] Kuchibholta R., Campbell J., Tsai C., *Internat. Conf. on InP and Related Compounds, Cardiff, April 8-13, 1991.*

[39] Campbell J. C., Chandrasekhar S., Tsang W. T., Qua G. J., Hohnson B. C., *J. Lightwave Technol.*, 7 (1989), 473.

[40] Zhang G., Hakkarainen T., Rakennus K., Tappura K., Asonen H., Pessa M., *Third Internat. Conf. on CBE Related Growth Techniques, Oxford, UK, Sept. 1-5, 1991.*

[41] Salokatve A., *Molecular Beam Epitaxy Technology for Quantum Well Devices*, Ph. D. Thesis, Tampere University of Technology. Publication 77, 1991.